Journal of Molecular and Cellular Cardiology Plus 5 (2023) 100046

Contents lists available at ScienceDirect

Journal of Molecular and Cellular Cardiology Plus

journal homepage: www.journals.elsevier.com/journal-of-molecular-andcellular-cardiology-plus

Genetic deletion of 12/15 lipoxygenase delays vascular remodeling and limits cardiorenal dysfunction after pressure overload

Dae Hyun Lee [a], Vasundhara Kain [a], Da-Zhi Wang [a], Donald G. Rokosh [b], Sumanth D. Prabhu [b], Ganesh V. Halade [a,*]

[a] Division of Cardiovascular Disease, Department of Internal Medicine, Morsani College of Medicine, University of South Florida, Florida 33602, United States
[b] Cardiovascular Division, Department of Internal Medicine, Washington University School of Medicine, MO 63110, United States

ARTICLE INFO

Keywords:
Heart failure
Inflammation-resolution signaling
Lipid mediators
Lipoxygenase
Pressure overload
Transverse aortic constriction

ABSTRACT

The lipid metabolizing enzyme 12/15 lipoxygenase (12/15LOX) induces proinflammatory responses that may increase cardiovascular and renal complications after cardiac insult. To define the role of 12/15LOX, 8–12-week-old male C57BL/6J wild-type (WT; $n = 49$) and 12/15LOX$^{-/-}$ mice ($n = 50$) were subject to transverse aortic constriction (TAC) and monitored for 7, 28, and 56 days (d) post-TAC. Compared with WT, 12/15LOX$^{-/-}$ mice experienced less left ventricle (LV) dysfunction with limited LV hypertrophy and lung edema post-TAC. 12/15LOX deletion decreased TAC-induced proinflammatory mediators 12-HETE and prostaglandins with modulation in mir-7a-5p, mir 26a-5p, miR-21e-5p, and miR-107-3p during chronic remodeling period (after d28). At d7 post-TAC, 12/15LOX$^{-/-}$ mice showed increased cardiac gene expression of *Arg-1* and the prostanoid receptors *EP2* and *EP4*. The *EP4* receptor expression was consistently elevated from d7 till d56 in 12/15LOX$^{-/-}$ mice post-TAC compared with WT controls. Post-TAC, wheat germ agglutinin staining revealed less cardiomyocyte hypertrophy at d28 and d56 in 12/15LOX$^{-/-}$ mice compared with WT. TAC-induced vascular remodeling was marked by disruption in the endothelium, evident by irregular CD31 staining and increased alpha-smooth muscle actin (α-SMA) in WT mice at d28 and d56. Compared to WT, 12/15LOX$^{-/-}$ mice exhibited a diminished expression of NGAL in the kidney, suggesting that 12/15LOX$^{-/-}$ reduced cardiorenal dysfunction post-TAC. In WT-TAC mice, structural analyses of the kidney revealed glomerular swelling during the maladaptive phase of heart failure, with decreases in the capsula glomeruli space and glomerular sclerosis compared to 12/15LOX$^{-/-}$ mice. Overall, vascular and kidney inflammation markers were higher in WT than in 12/15LOX$^{-/-}$ post-TAC. Thus, deletion of 12/15LOX limits LV hypertrophy associated with perivascular inflammation and cardiorenal remodeling after pressure overload. Deficiency of 12/15 LOX serves a dual role in delaying an early adaptive interstitial remodeling with long-term protective effects on cardiac hypertrophy and cardiac fibrosis and detrimental adverse vascular remodeling during later maladaptive remodeling after pressure overload.

1. Introduction

Cardiovascular disease is the leading cause of death in the United States and worldwide [1,2]. The progression of various cardiovascular diseases may eventually lead to heart failure. Heart failure is a clinical disease characterized by volume and pressure overload secondary to myocardial dysfunction [3]. Chronic, low-grade inflammation plays an important role in the development of heart failure [4–8]. Transverse aortic constriction (TAC) is one of the pre-clinical model for the non-ischemic cause of heart failure secondary through exerting pressure overload in the aorta [9]. Multiple studies have identified the role and interaction of specific immune cells on the development of adverse cardiac remodeling after TAC [10–13].

Until recently, the progression of inflammation was thought to be of two types: pro-inflammatory and anti-inflammatory pathways. In the past, the inflammation-resolution axis was thought to be mediated predominantly by the anti-inflammatory pathway via blockage and inhibition of pro-inflammatory mediators [4]. However, a novel pathway, collectively called the resolution pathway, is mediated through lipid mediators such as specialized pro-resolving mediators (SPM, e.g.,

* Corresponding author at: Division of Cardiovascular Sciences, Department of Internal Medicine, Heart Institute, Morsani College of Medicine, University of South Florida, 560 Channelside Dr, Tampa, FL 33602, United States.
E-mail address: ghalade@usf.edu (G.V. Halade).

https://doi.org/10.1016/j.jmccpl.2023.100046
Received 6 July 2023; Received in revised form 16 August 2023; Accepted 16 August 2023
Available online 19 August 2023

lipoxins, resolvins, and protectins). Lipid mediators are derived from free fatty acids and produced by various enzymes such as lipoxygenase (LOX), cyclooxygenase (COX), or cytochrome P450 epoxygenase (CYP) [4,14]. SPMs exert safe clearance of inflammation, termed as the resolution of inflammation produced by 12/15LOX, but it also produces pro-inflammatory lipid mediators such as 12(*S*)-HETE that triggers residual inflammation and subsequent heart failure [15]. Different types of LOX (5, 12, or 15) have an active role in the outcome of obesity, diabetes, atherosclerosis, and ischemic cardiomyopathy in pre-clinical models [16–19]. 12/15LOX is constitutively expressed in a wide range of tissues such as reticulocytes, eosinophils, dendritic cells, alveolar macrophages, immature dendritic cells, vascular cells, and resident peritoneal macrophages [20]. Peripheral blood monocytes from humans and mice do not naturally express 12/15-LOX, however, IL-4 and IL-13 can do so in vitro in human monocytes and murine macrophages [21]. In addition, 12/15 LOX levels are increased in atherosclerosis and acute coronary syndrome in humans [22]. We have previously shown the beneficial effect of 12/15 LOX deletion on post-myocardial infarction (MI) by promoting reparative macrophages and limiting cardio-renal inflammation [17]. As suppression of 12/15 LOX led to enhancement of inflammation resolution in MI, we have investigated the role of 12/15 LOX deletion in another pre-clinical model of heart failure using the TAC-mediated pressure overload in adaptive and maladaptive cardiac remodeling. Our results suggest that deletion of 12/15LOX limits LV hypertrophy associated with perivascular inflammation and cardiorenal remodeling, however drives vascular remodeling in chronic heart failure after pressure overload.

2. Methods

2.1. Animal care compliance

All animal procedures were conducted according to the "Guide for the Care and Use of Laboratory Animals" (8th Edition. 2011) and "AVMA Guidelines for the Euthanasia of Animals" (2013 Edition). The Institutional Animal Care and Use Committees approved the study at the University of Alabama, Birmingham, and The University of South Florida, Tampa, USA.

2.2. Mice and transverse aortic constriction surgery (TAC)

8–12 weeks male C57BL/6 (wild type; WT $n = 49$) and 12/15 LOX null mice (12/15LOX$^{-/-}$; $n = 50$) on the C57BL/6 genetic background were obtained from The Jackson Laboratory (Bar Harbor, Maine, USA) and were maintained under constant temperature (19.8–22.2 °C). The mice were given free access to water and a standard chow diet. Mice were subject to TAC under 1.5–2 % isoflurane in a 100 % oxygen mix anesthesia. Animals were placed in the supine position, and a midline cervical incision was made to reach the trachea and carotid arteries to facilitate intubation. Following intubation, the chest cavity is entered in the second intercostal space at the upper sternal area with a small incision, and aortic constriction is achieved by clamping the aortic arch at 0.4 mm diameter [9,23].

2.3. Echocardiography

For the echocardiography data acquisition, mice were anesthetized using 3–4 % and then maintained anesthesia using 1.0–2.0 % isoflurane in a 100 % oxygen mix. Electrocardiograms and heart rates were monitored using a surface electrocardiogram. Echocardiographic images were acquired using the Vevo 3100 imaging systems (Visual Sonics) equipped with probes up to 18–38 MHz (3100). Short and long-axis images were acquired at heart rates >400 beats/min to achieve physiologically relevant measurements. Measurements were taken from the two-dimensional parasternal long-axis (B-mode) and short-axis (M-mode) recordings from the mid-papillary region. Echocardiograms were performed before the necropsy for the day (d) 0 control mice and d7, d28, and d56 post-TAC mice. Data from Vevo 3100 imaging system was analyzed using strain analysis software on the parasternal long-axis B-mode images to automatically calculate left ventricle (LV) end-diastolic and systolic volumes (ESV, EDV), cardiac output (CO), fractional area shortening (FAC) and ejection fraction (EF). These calculated measurements were reinforced with manual wall thickness measurements and fractional shortening using 3 consecutive cardiac cycles for M-mode short-axis images [15,24].

2.4. Necropsy

Naïve control day (d0) and post-TAC d7, d28, or d56 mice were anesthetized under isoflurane briefly, then mice were maintained under anesthesia using 2 % isoflurane in 100 % oxygen mix, and heparin (4 IU/g) was injected. The blood was collected from the carotid artery for plasma separation. The chest cavity was opened, and the left ventricle was perfused with 2–3 ml cardioplegic solution. The heart, lungs, and kidneys were then removed. The lungs, LV, right ventricle, and kidneys were separated and weighed individually. The LV was divided into apex (molecular biology analysis), mid-cavity (histology), and base (molecular biology analysis) under the microscope. The apex and base regions were separated under the microscope for precise separation and were snap-frozen with liquid nitrogen and stored at −80 °C. The mid-cavity section was fixed in 10 % zincformalin and paraffin-embedded for histological examination. The left kidney is removed and sliced along the longitude, with one half placed in zinc formalin. The right kidney is snap-frozen and stored at −80 °C for molecular analysis. The lungs and tibia were removed, and the wet and dry weights of the lungs (24 h after necropsy) and the tibia length were determined [15].

2.5. Histology staining

For immunohistochemistry (IHC), the LV mid-cavity section and half kidney were embedded in paraffin and sectioned at 5 μm. For picrosirius red (PSR) staining, paraffin-embedded unstained LV and kidney tissue sections were deparaffinized in Citrisolve (Fisher) and rehydrated through subsequent ethanol washes. After a wash with water, phosphomolybdic acid (0.2 % in water) was placed on the section. Sirius red was added by a subsequent wash with water, 0.1 % in saturated picric acid (26357-02), and then the application of 0.01 N hydrochloric acid. Then, the slides were dehydrated and mounted using permount. The slides were allowed to dry for image acquisition and analysis. Periodic Acid Schiff (PAS) staining was performed on the left ventricle and kidney sections. Paraffin-embedded, unstained cuts of LV and kidney were deparaffinized in citrisolve (Fisher) and rehydrated with ethanol washes. Slides are then circumscribed using an Immedge Pen (Vector), treated with 0.5 % periodic acid (Fisher CAS 10450-60-9), and washed with distilled water. Slides were then treated with Schiff reagent (Fisher) for 15 min, followed by 1 min of 0.55 % potassium metabisulfite (Fisher CAS 16731-55-8) to remove excess stain. Slides are washed with running tap water and counterstained for 30 s with Harris hematoxylin solution. The slides are dehydrated with washes of increasing ethanol concentration and Citrisolve before being mounted with coverslips using permount (Biocare medical "EcoMount") [15,16].

2.6. Histology image analysis

For each slide per mouse, 5–7 images were captured focusing on perivascular and interstitial areas using a microscope (BX43) with an attached camera (Olympus DP73). The images were captured using the cellSens Dimension program (Olympus version 1.9). For the kidney PAS analysis, 40× images focusing on the glomeruli were captured and analyzed using the EGTI (Endothelial, Glomerulus, Tubular, Interstitial) scoring system to assess kidney damage. PSR staining of LV was captured using a plane-polarized light filter, allowing collagen from PSR to be

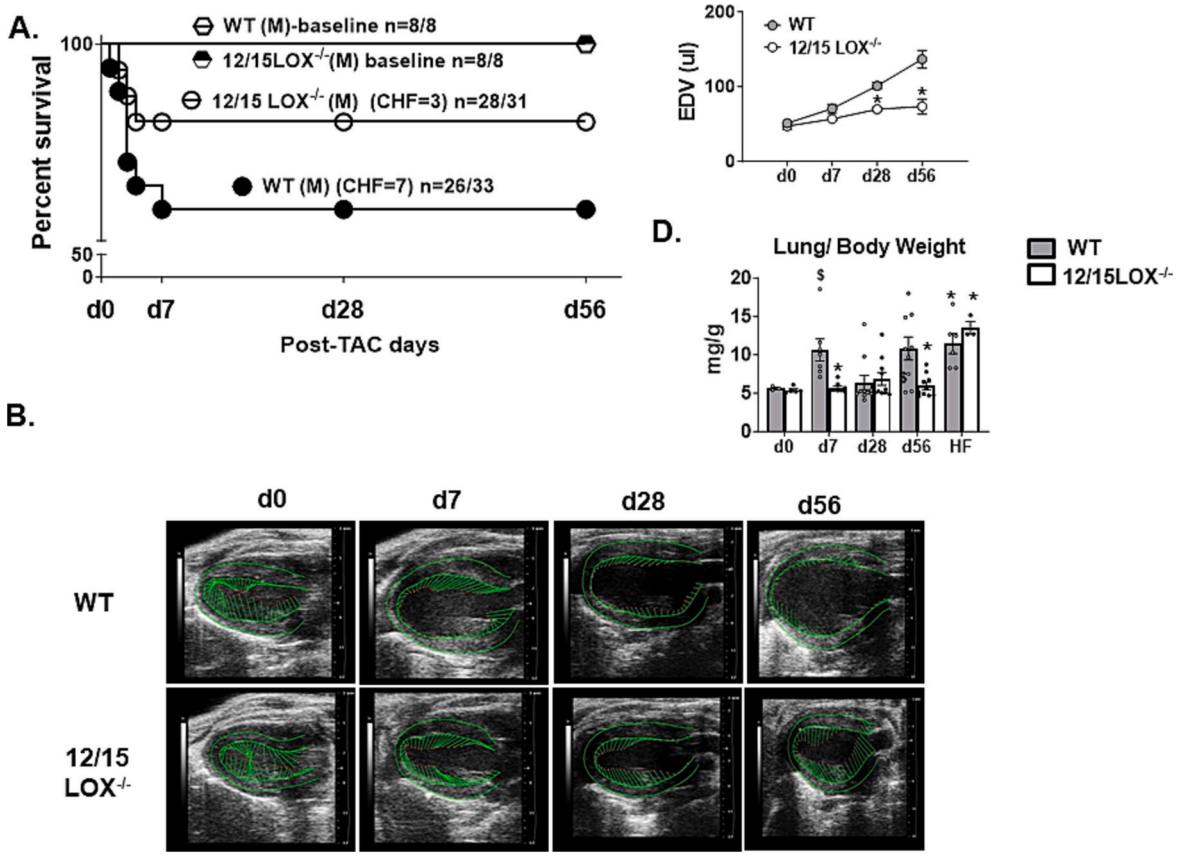

Fig. 1. Deletion of 12/15 LOX in mice leads to reduced LV dysfunction, LV remodeling, and limited lung edema in the TAC-induced pressure overload model. **A.** Kaplan Meier Survival curve shows similar survival of 12/15LOX$^{-/-}$ mice versus WT mice post–TAC (WT, *n*=26/33; 12/15LOX$^{-/-}$, *n*=28/31), base line mice for each genotype, *n*=8. **B.** Representative image of parasternal long axis LV showing decreased systolic function and strain of WT mice compared to 12/15LOX$^{-/-}$ mice post-TAC. **C.** Repeated measures line graph for end diastolic volume (EDV) in WT and 12/15LOX$^{-/-}$ mice until d56. Data information: Comparisons between groups at time points were done using ordinary two-way ANOVA with multiple-comparisons test *$p < 0.05$. (Number of mice for WT at various timepoints d0, *n*=14; d7, *n*=11; d28, n=14; d56, *n*=10. Number of mice for 12/15LOX$^{-/-}$ at the following timepoints: d0, n=11; d7, n=11; d28, n=14; d56, n=14). **D.** Bar graph of wet lung weight normalized to body weight at different time points. Data information: Comparisons between groups at time points were done using ordinary two-way ANOVA with multiple-comparisons test "*" indicates $p < 0.05$ vs. WT at day 0; "$" indicates $p < 0.05$, when compared to 12/15LOX$^{-/-}$ at day 0. Error bars represent mean ± SEM; (Number of mice for WT at the following timepoints: d0, *n*=5; d7, *n*=7; d28, n=10; d56, n=11, Number of mice for 12/15LOX$^{-/-}$ at the respective timepoints: d0, n=5; d7, n=8; d28, n=10; d56, *n*=12).

Table 1
Necropsy parameters indicating reduced LV remodeling in 12/15LOX$^{-/-}$ mice post-TAC surgery.

	Naïve control		Transverse aortic constriction					
	Day 0		Day 7		Day 28		Day 56	
Necropsy parameters	WT	12/15LOX$^{-/-}$	WT	12/15LOX$^{-/-}$	WT	12/15LOX$^{-/-}$	WT	12/15LOX$^{-/-}$
n	5	5	7	8	10	10	11	12
Body weight (g)	22±1	24±1	23±1	22±1	26±1	23±1	27±1	25±1
LV (mg)	72±2	74±3	122±12*	103±7	133±9*	122±6*	164±8*	126±7$^{\$}$*
LV/BW (mg/g)	3.3±0.1	3.2±0.1	5.4±0.6*	4.6±0.2	5.0±0.2*	5.2±0.2*	6.2±0.4*	5.0±0.3*
LV/Tibia	4.3±0.1	4.4±0.2	7.2±0.6*	6.1±0.3	7.9±0.5*	7.1±0.4*	9.4±0.4*	7.3±0.4$^{\$}$*
Lung weight (mg)	146±18	127±7	198±43	127±7	170±29	161±21	217±29*	150±9
Tibia(mm)	16.7±0.2	16.7±0.7	17.0±0.2	16.9±0.2	16.9±0.2	17.2±0.1	17.5±0.1	17.3±0.2

Values are mean ± SEM. n indicates mice sample size/group; LV, Left ventricle; BW, body weight *p<0.05 vs the day 0 control, $p<0.05 vs WT at the respective time point.

viewed in shades of yellow and green that distinguish between type I and type III collagen [15].

2.7. Quantitative mass spectroscopy analyses of left ventricular lipid metabolites

A targeted quantitative mass spectroscopy approach was used to detect the lipid metabolites in WT and 12/15LOX$^{-/-}$ mice in naïve controls and post-TAC, as previously described [25,26].

2.8. Measurements of mRNA levels using quantitative real-time PCR

For quantitative RT-PCR, reverse transcription was performed with 2.5 μg total RNA using SuperScript VILO cDNA synthesis kit (Invitrogen, Carlsbad, CA). Quantitative RT-PCR for (EP2, EP4, Ccl2, TNF-α, Arg-1, and Mrc-1 in LV and NGAL and TREM in kidney) genes was

Table 2
Echocardiography results suggesting reduced rate of heart failure progression in 12/15LOX$^{-/-}$ mice compared to WT post-TAC.

Groups/echocardiography parameters	Naïve control		Transverse aortic constriction					
	Day 0		Day 7		Day 28		Day 56	
	WT	12/15LOX$^{-/-}$	WT	12/15LOX$^{-/-}$	WT	12/15LOX$^{-/-}$	WT	12/15LOX$^{-/-}$
n	14	11	11	11	14	14	10	14
Heart rate (bpm)	445±10	436±9	419±21	410±40	437±17	424±18	496±10	458±12
EDD (mm)	3.61±0.09	3.62±0.01	4.1±0.1	3.7±0.1	4.1±0.1	4.1±0.1	4.8±0.1*	4.1±0.1
ESD (mm)	2.42±0.11	2.33±0.12	3.3±0.2	2.6±0.1	3.4±0.1	3.1±0.1	4.2±0.1	3.2±0.1
EDV (μl)	63±5	51±4	54±18	55±2	84±6*	67±3*$^{\$}$	97±10*	65±4$^{\$}$
ESV (μl)	27±5	29±6	29±12*	31±2	54±4*	43±3$^{\$}$	73±10*	39±3$^{\$}$
FS(%)	35±1	36±1	20±2*	30±1*$^{\$}$	18±1*	23±2*$^{\$}$	13±1*	22±2*$^{\$}$

Values are mean± SEM; n indicates sample size/group. bpm, beats per minute; ESV, end-systolic volume; EDV, end-diastolic volume; EDD, end-diastolic dimension; ESD, end-systolic dimension; FS, fractional shoestening; mm, millimeter;%; percentage. *p< 0.05 vs. day 0 wild-type (WT) control; $$p$< 0.05 vs. WT at respective time point.

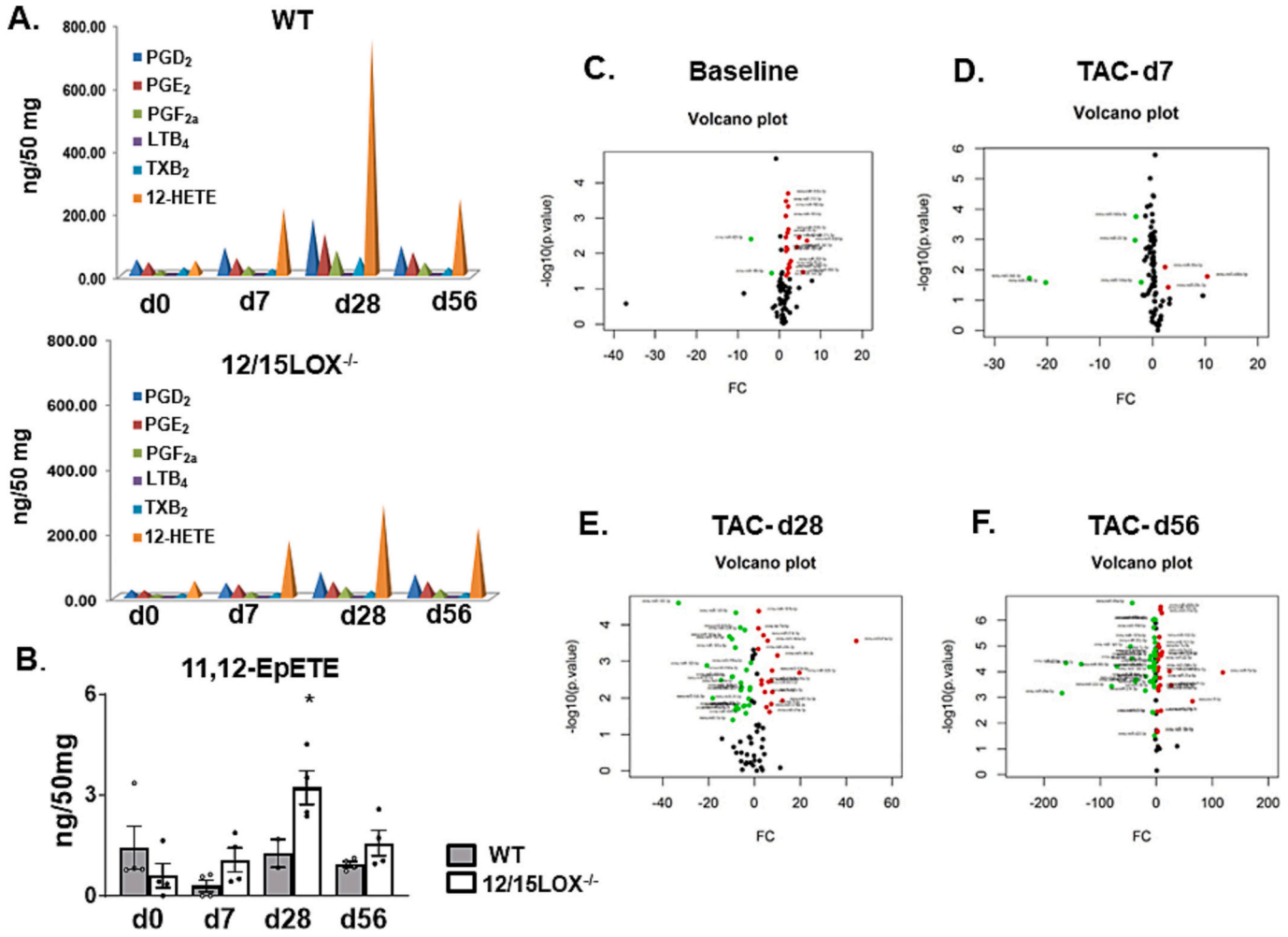

Fig. 2. Deletion of 12/15 LOX reduces prostaglandin and 12-HETE with changes in miRs in the TAC-induced pressure overload model.
A. Cone graphs displaying quantified bioactive proinflammatory lipid mediators (PGs, TXs, LTB4, and 12HETE) in WT and 12/15LOX$^{-/-}$ LV at baseline and post-TAC day 7 to day 56. Quantification and values are pg/50 mg of LV tissue (WT: n=4 and 12/15LOX$^{-/-}$: n=4). The detection limit was ~1 pg. Quality controls (QC) are done for lipidomic analysis. **B.** Bar graph displays 11,12-EpETEs levels in WT and 12/15LOX$^{-/-}$ hearts at baseline and post-TAC. Data information: Comparisons between groups at time points were done using ordinary two-way ANOVA with a multiple-comparisons test. * indicates p < 0.05 vs WT at each respective timepoint. Values represent mean ± SEM; (Number of mice for WT at respective timepoints: d0, n=4; d7, n=4; d28, n=4; d56, n=4. Number of 12/15LOX$^{-/-}$ for respective timepoints: d0, n=4; d7, n=4; d28, n=4; d56, n=4). **C–F.** Volcano plot displaying miRNAs expression in 12/15LOX$^{-/-}$ heart in baseline control samples and post-TAC samples. The x-axis is $\log_2$ fold-change, and the y-axis is log fold change. In each graph, every point represents an individual transcript. The upregulated (right, red dots) and downregulated (left, green dots) miRs are shown. (For interpretation of the references to color in this figure legend, the reader is referred to the web version of this article.)

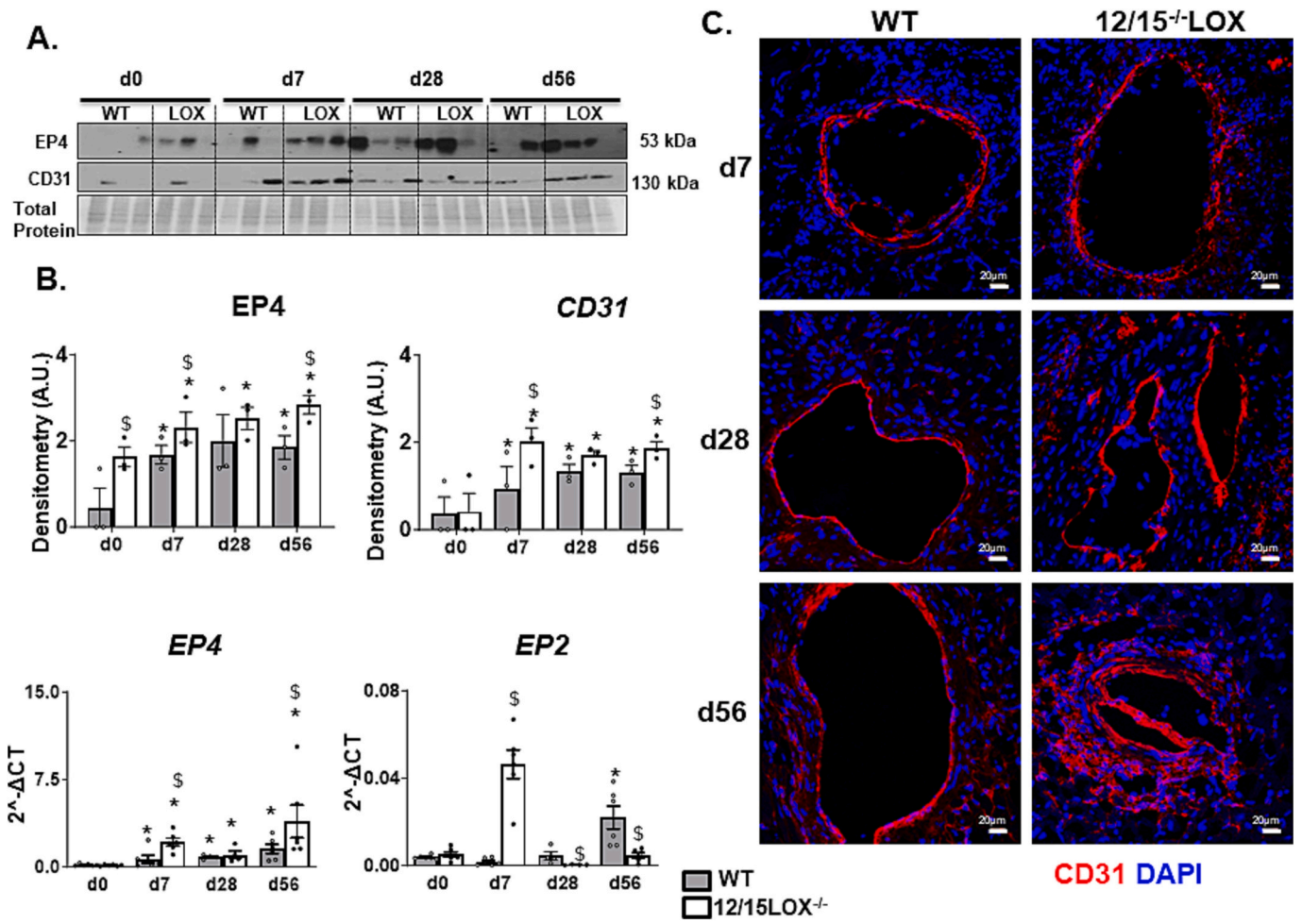

Fig. 3. Deletion of 12/15 LOX leads to an increased level of EP4 in heart and CD31 in vessel following pressure overload.
A. Immunoblot showing the level of EP4 and CD31 at different time points after TAC. **B.** Bar graph of protein densitometry (AU) of EP4 and CD31 and mRNA level changes ($2^{-\Delta CT}$) of EP4 and EP2. Values are represented as mean ± SEM; n=4 mice/group/day. *$p<0.05$ compared to baseline; \$$p<0.05$ compared to WT control at respective time points. **C.** Representative immunofluorescence images of CD31 expression (red) in the left ventricle at different time points in 12/15 $LOX^{-/-}$ mice and WT. Nuclei stained with DAPI (blue). Magnification at 40× and scale bar indicates 20 μm. Images are representative of 5–8 fields/slides. n=4 individual mouse slides/group. (For interpretation of the references to color in this figure legend, the reader is referred to the web version of this article.)

performed using TaqMan probes (Applied Biosystems, Foster City, CA) on master cycler ABI, 7900HT. Gene levels were normalized to hypoxanthine phosphoribosyltransferase as the housekeeping control. The results were reported as $2^{-\Delta\Delta Ct}$ (ΔΔCt) values (where Ct is the threshold cycle). All experiments were duplicated with $n = 5$–9 mice per group per time point.

2.9. miRNA array profiling

Micro RNA (miRNA) gene expression profiling was performed using miRNA PCR arrays in frozen LV tissue per the manufacturer's instructions and previous reports [16]. In brief, miRNAs were isolated with the miRNeasy Mini Kit (217,004; Qiagen, Germantown, MD, USA), and cDNA synthesis was performed with miScript II RT Kit (Qiagen). Each sample was loaded on the RT2-PCR plate (mi-Script miRNA PCR array MIMM-113ZE-4; Qiagen) and was run on an ABI 7900HT PCR system (Thermo Fisher Scientific). The results were reported as $2^{-\Delta\Delta Ct}$ values.

2.10. LV protein extraction and immunoblotting

Protein extraction and immunoblotting for EP4 and CD31 on LV tissues pre- and post-TAC were performed as described previously [16]. The total protein lane was used as an internal loading control. Image J was used for densitometry analysis as previously described [27].

2.11. Confocal microscopy

The confocal microscopy was performed on LV mid-cavity, using α-SMA (sigma) was done as previously described. Alexa Fluor®, 488 conjugate of WGA (wheat gram agglutinin), was used to measure the area of cardiomyocyte as previously described [17]. TUNEL staining on LV and kidney tissues was done using DeadEnd™ Fluorometric TUNEL System (Promega #G33250) as per the manufacturer's instruction. The images were acquired on Nikon A1 and Keyence microscope.

2.12. Statistical analysis

Data were expressed in mean ± standard error of the mean (SEM) and bar graph with SEM. ANOVA with posthoc Newman-Keuls test was performed to compare groups. Kaplan Meier and log-rank tests were performed to compare survival between groups. P-value <0.05 was considered statistically significant. All statistical analysis was performed with GraphPad Prism.

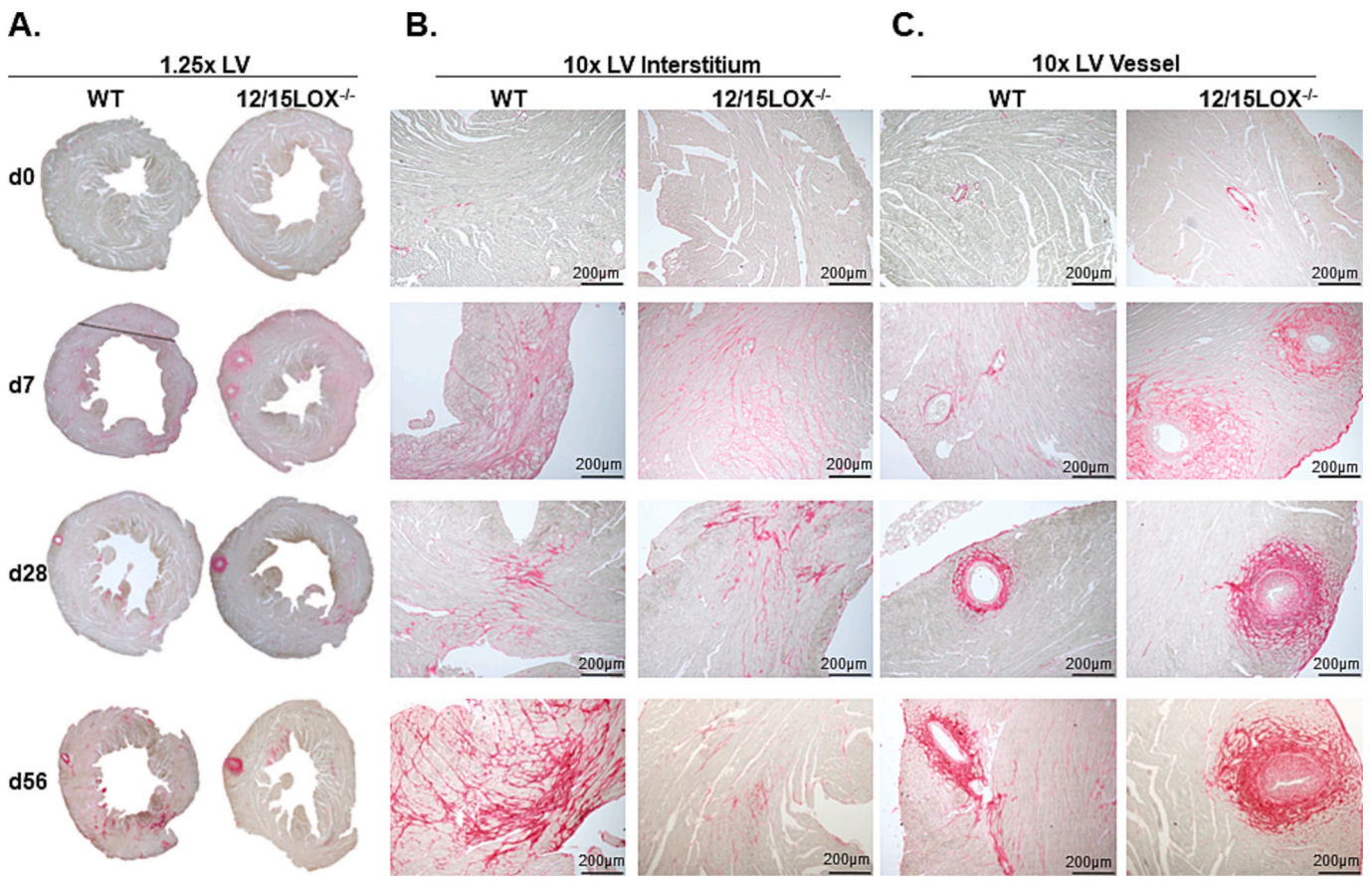

Fig. 4. Deletion of 12/15 LOX limits LV interstitial fibrosis but promotes perivascular and neointimal fibrosis compared to WT in pressure overload induced by TAC. **A.** Representative 1.25× LV images show dilation and hypertrophy after TAC. **B.** Picrosirus red-stained LV images indicated delayed fibrosis in 12/15LOX$^{-/-}$ mice. 10× scale bar indicates 200 μm accompanied with1.25× images. Images are representative of 5 fields/slides. n=4 individual mouse slides per group. (For interpretation of the references to colour in this figure legend, the reader is referred to the web version of this article.)

3. Results

3.1. 12/15LOX deletion reduces progression to heart failure with improved LV function, and lung edema

Cardiac pressure overload through TAC was performed in 12/15 LOX deletion mice to evaluate adaptive and maladaptive cardiac remodeling. Both 12/15LOX$^{-/-}$ and WT mice have a similar survival rate (Log Rank test Chi-square 0.47, p=0.49) (Fig. 1A). Echocardiography and necropsy data indicate that 12/15LOX deletion had improved cardiac function and volume (EDV and ESV) as early as day 28 post-TAC compared with WT (Fig. 1C–D and Tables 1–2). Furthermore, 12/15LOX deletion had lower heart weight and decreased pulmonary edema than WT (Fig. 1E and Table 1). Overall, these findings suggest a role for 12/15LOX in the late maladaptive cardiac remodeling process following pressure overload.

3.2. 12/15LOX deletion limits pro-inflammatory mediators such as 12-HETE, and prostaglandins

To determine 121/5LOX-specific targeted mediators, a total of 139 bioactive lipid mediators (both enzymatic and non-enzymatic) were analyzed quantitatively using mass spectrometry in WT and 12/15LOX$^{-/-}$ mice LV to determine the impact of TAC. As a result of pressure overload, prostaglandins (PGs) PGD_2, PGE_2 and PGF_{2a}, and 12-HETE were increased in WT LV. These lipid mediators levels were highest at d28 post-TAC and declined at d56. The 12/15LOX deletion reduced both PGs and 12-HETE after TAC from d7 to d56 (Fig. 2A). In contrast, the 11,12-EpETE level was increased in d28 post-TAC in 12/15 LOX deletion (Fig. 2B). Thus, 12/15LOX deletion controls pro-inflammatory mediators thereby limited early cardiac remodeling.

3.3. 12/15LOX deletion leads to time-dependent changes in miRNA

To understand the temporal effect of 12/15LOX deletion after TAC on miRNA changes, we performed a comprehensive analysis of the set of miRNA (Supplemental Table 1). miRNA expression by volcano plot revealed that 12/15LOX deletion at baseline modulated 22 types of miR, out of which 20 were upregulated and 2 were downregulated (Fig. 2C). During the early, adaptive remodeling phase (TAC d7), only 8 miRNA were significantly changed (3 upregulated: miR-30e-5p, miR-486b-5p, and miR-29c-3p and 5 downregulated: miR-342-3p, miR-295-3p, miR-142-3p, miR-22-3p, and miR-145a-5p) (Fig. 2D). In contrast, at the beginning of the maladaptive remodeling phase (TAC d28), 45 miRNAs were significantly changed, out of which 19 were upregulated and 26 were downregulated. Most significant changes occurred in miR-21e-5p (upregulated ~40 fold) and miR-107-3p (downregulated ~35 fold) (Fig. 2E) in 12/15LOX$^{-/-}$ mice. Similarly, during the chronic, late maladaptive period (post-TAC d56), 22 miRs were upregulated, and 37 miRs were downregulated in 12/15 LOX$^{-/-}$ mice (Fig. 2F). Overall, 12/15LOX deletion led to various miRNA-directed transcriptional changes in an early and late cardiac remodeling following pressure overload.

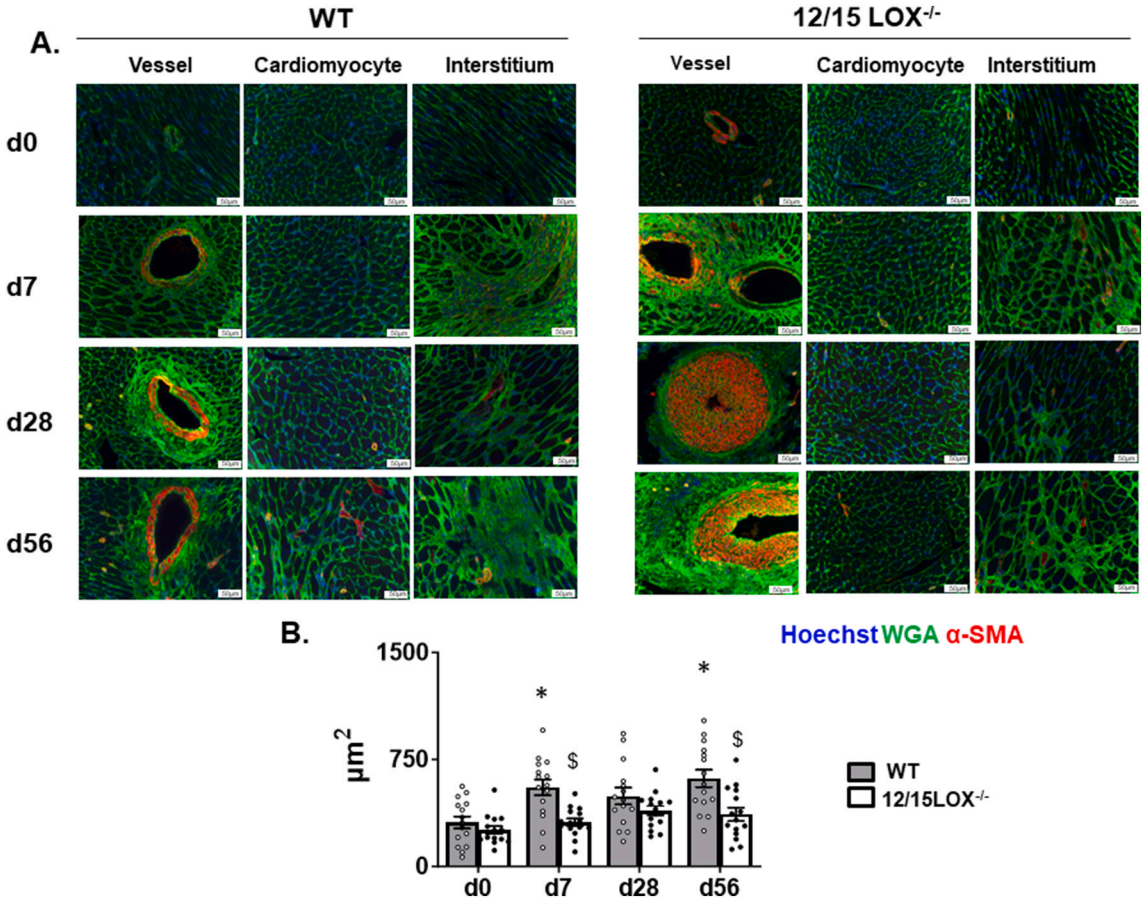

Fig. 5. Deletion of 12/15LOX leads to less cardiomyocyte hypertrophy in pressure overload induced by TAC.
A. Representative immunofluorescence images of cardiomyocyte as stained by WGA (wheat germ agglutinin-green) and α-SMA (α-smooth muscle actin-red) in the left ventricle of WT and 12/15LOX null mice at different time points post-TAC. Nuclei are labeled with Hoechst (blue) Magnification at 40× and the scale bar indicates 50 μm. Images are representative of 4 fields/slides. *n*=4 slides per group. **B.** Bar graph of cardiomyocyte area in LV of WT and 12/15LOX null mice from d0 to post-TAC d7 to d56 points. For area calculation minimum of 20 cardiomyocytes are counted in an area. For calculation, at least 5 areas are taken for counting from a single slide. Data information: Comparisons between groups at time points were done using ordinary two-way ANOVA with a multiple-comparisons test. Values represent mean ± SEM * $p<0.05$ compared to baseline; $p<0.05 compared to WT control at respective time points. (WT: d0, *n*=4; d7, n=4; d28, n=4; d56, n=4, 12/15LOX$^{-/-}$: d0, n=4; d7, n=4; d28, n=4; d56, n=4). (For interpretation of the references to color in this figure legend, the reader is referred to the web version of this article.)

3.4. Protein expression of EP2 and EP4 are increased in 12/15 LOX deletion

We have previously shown that 12/15LOX deletion directs towards early, protective cardiac remodeling after MI through E-type prostanoid receptor activation [16]. Therefore, we assessed the changes in gene transcript of EP2 and EP4 after TAC. The protein and mRNA levels of EP4 and CD31 were increased post-TAC d7 to d56 in WT. In 12/15LOX$^{-/-}$ mice, the expression of EP4 and CD31 in the LV was higher than WT after TAC. While the EP4 expression peaked later at d56, CD31 peaked earlier at d7 post-TAC in 12/15LOX$^{-/-}$ mice. (Fig. 3A–B) The CD31 expression was localized to intramyocardial vessels of LV, with a more irregular staining pattern in 12/15LOX$^{-/-}$ mice post-TAC (Fig. 3C).

3.5. 12/15 LOX deletion reduces interstitial fibrosis and cardiomyocyte hypertrophy with increased maladaptive peri-vascular remodeling

In response to pressure-overload-triggered hypertrophic remodeling, temporal changes such as progressive interstitial collagen deposition and vascular hypertrophy occur (Fig. 4A). As assessed by PSR staining, the interstitial fibrotic remodeling was more severe in WT-LV compared to 12/15LOX$^{-/-}$ mice after d7 post-TAC (Fig. 4B). Likewise, overall vascular remodeling, as measured by the area of the vessel within the external elastic lamina, had a different overall morphology in 12/15LOX$^{-/-}$ mice during adaptive remodeling at d7 post-TAC with higher peri-vascular collagen deposition around the vessel in 12/15LOX$^{-/-}$ mice. The lumen area was smaller in 12/15LOX$^{-/-}$ vessels after TAC during maladaptive remodeling (post-TAC d28 and d56), with a concomitant increase in collagen density of perivascular region (Fig. 4C). In addition, wheat germ agglutinin (WGA) and α-SMA (alpha-smooth muscle actin) staining showed less cardiomyocyte hypertrophy and lower α-SMA at d56 post-TAC in 12/15 LOX$^{-/-}$ mice (Fig. 5A) but decrease in the intimal area (Fig. 5B). Our results suggest that 12/15LOX deletion decreased cardiac hypertrophy and limited interstitial fibrosis in adaptive remodeling however, reduced lumen area as a sign of neo-intimal formation with increased perivascular fibrosis in maladaptive remodeling following pressure overload.

3.6. 12/15 LOX deletion reduced LV apoptosis post-TAC without impacting cytokine markers

To provide insight into the underlying mechanisms for inflammation and remodeling early after TAC, we measured RNA levels of cytokine mediators in LV, such as C-C Motif Chemokine Ligand 2 (CCL2), tumor necrosis factor-α (TNF-α), Arginase-1 (Arg-1) and Mannose Receptor C-Type 1 (MRC-1). In early remodeling (d7 TAC), there was an increase in

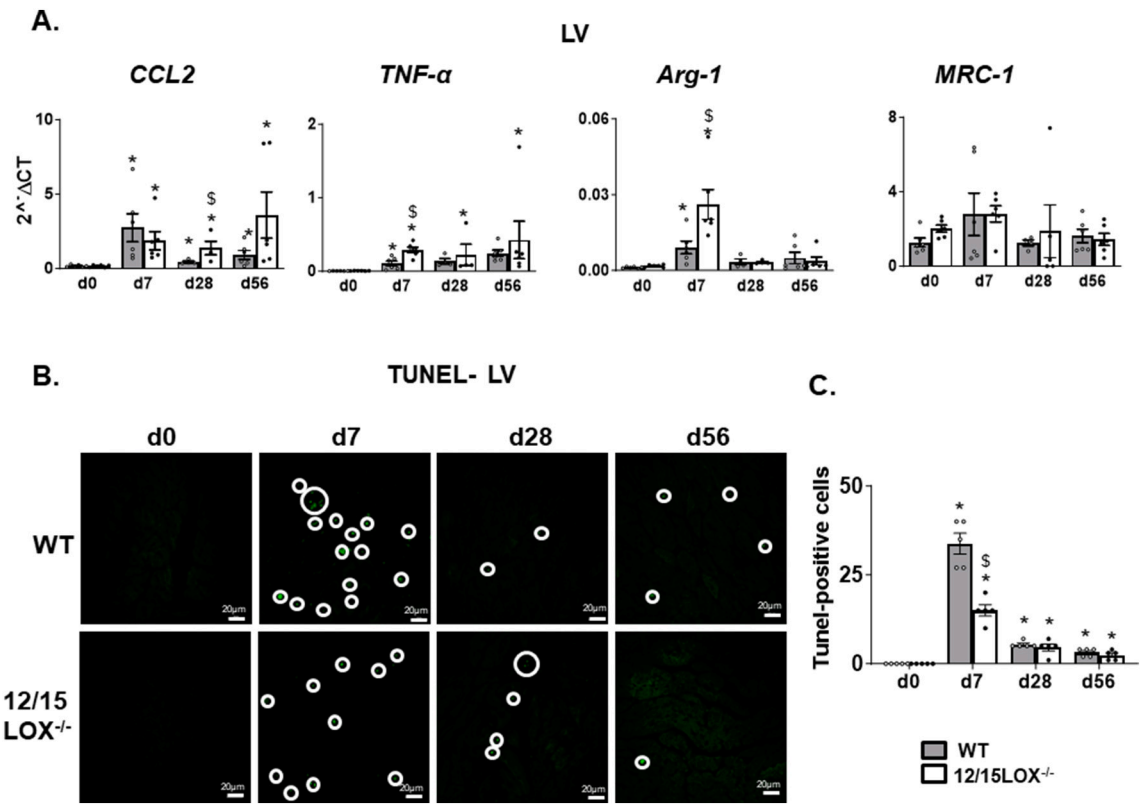

Fig. 6. Deletion of 12/15 LOX leads to decreased LV apoptosis in pressure overload induced by TAC.
A. Bar graph displaying mRNA expression of *CCL2*, *TNF-α*, *Arg-1*, and *MRC-1* in LV at different time points. mRNA levels were normalized to hypoxanthine phosphoribosyltransferase 1 (HPRT-1). Data information: Comparisons between groups at time points were done using ordinary two-way ANOVA with multiple-comparisons test *$p< 0.05$ vs WT at respective day. Values represent mean ± SEM; (Number of mice WT: d0, n=4; d7, n=4; d28, n=4; d56, n=4. Number of mice 12/15LOX$^{-/-}$: d0, n=4; d7, n=4; d28, n=4; d56, n=4). **B.** Representative image of TUNEL staining in LV at d7, d28, and d56 post-TAC representing a decrease in apoptotic cells (TUNEL positive cell: green) in 12/15LOX$^{-/-}$ mice, compared with WT mice (magnification 40×, scale bar indicates 20 μm). Images are representative of 8 fields/slide. n=4 individual mouse slides/group. **C.** Bar graph representing TUNEL positive cells. Data information: Comparisons between groups at time points were done using ordinary two-way ANOVA with a multiple-comparisons test. Values represent mean ± SEM. * $p<0.05$ compared to baseline; $p<0.05$ compared to WT control at respective time points. (For interpretation of the references to color in this figure legend, the reader is referred to the web version of this article.)

the expression of CCL2, TNF-α, Arg-1, and MRC-1 in WT. There was a concomitant increase in TNF-α, from d7 to d56, but the expression levels of CCL2, Arg-1, and MRC-1 were reduced in WT. The 12/15LOX deletion consistently increased the CCl2 and TNF-α d7 levels to d56 post-TAC. However, Arg-1 was increased significantly at d7 in 12/15LOX$^{-/-}$ mice with no change in MRC-1 levels compared to WT (Fig. 6A). To evaluate how 12/15LOX deletion regulated TAC-induced apoptosis during adaptive and maladaptive remodeling in LV, the TUNEL methodology was used. The representative LV section shows apoptotic nuclei in WT were highest at d7 during adaptive remodeling (d7) but decreased during maladaptive remodeling (d28, d56 post-TAC). The number of apoptotic nuclei in LV were lower in 12/15 LOX$^{-/-}$ mice than in WT, suggesting reduced early adaptive remodeling. Long-term follow-up up to d56 post-TAC shows that both groups have a similar number of apoptotic nuclei during later stages (Fig. 6B–C). Thus, our results suggest that 12/15LOX deletion modulated cardiac apoptosis during adaptive response but had a limited impact on cytokine markers in maladaptive remodeling following pressure overload.

3.7. 12/15LOX deletion suppressed the kidney inflammation in hypertrophic remodeling

In physiologic conditions, there is continuous crosstalk between the heart and kidney. Adverse cardiac remodeling leads to kidney injury, such as cardiorenal syndrome. Thus, we determined the level of kidney inflammation during adaptive and maladaptive stages of cardiac remodeling between WT and 12/15LOX$^{-/-}$ mice. To confirm whether TAC-induced apoptosis in the kidney, the TUNEL staining was used. The representative kidney section shows a higher number of apoptotic nuclei at d7, which decreased at d28 and d56 post-TAC in the WT kidney. The number of apoptotic nuclei was lower in 12/15LOX$^{-/-}$ kidneys (Fig. 7A-B). To determine whether there is an early impact on immune response due to cardiac remodeling in the kidney, we determined mRNA expression of innate immune system amplified Trem-1 (Triggering receptor expressed on myeloid cells 1). Trem-1 levels increased kidney during the adaptive phase in WT but started decreasing during d28-d56 post-TAC. However, Trem-1 expression was lower in 12/15LOX$^{-/-}$ kidneys at all stages than in their respective WT (Fig. 7C). The renal inflammation was confirmed by the early upregulation of neutrophil gelatinase-associated lipocalin (NGAL) in the kidney. The NGAL expression remains elevated in WT kidneys from TAC d7 to d56. However, the 12/15LOX$^{-/-}$ kidneys have lower NGAL expression from TAC d7 to d56 comapred with their respective WT control (Fig. 7D). Renal microstructure assessed by histology displayed limited mesangial expansion in glomeruli suggesting reduced glomerulonephritis in 12/15LOX$^{-/-}$ mice during the progression of hypertrophic remodeling (TAC d56) compared with WT mice (Fig. 7E). Thus, renal inflammation and apoptosis are reduced in 12/5LOX$^{-/-}$ mice during acute and chronic hypertrophic remodeling.

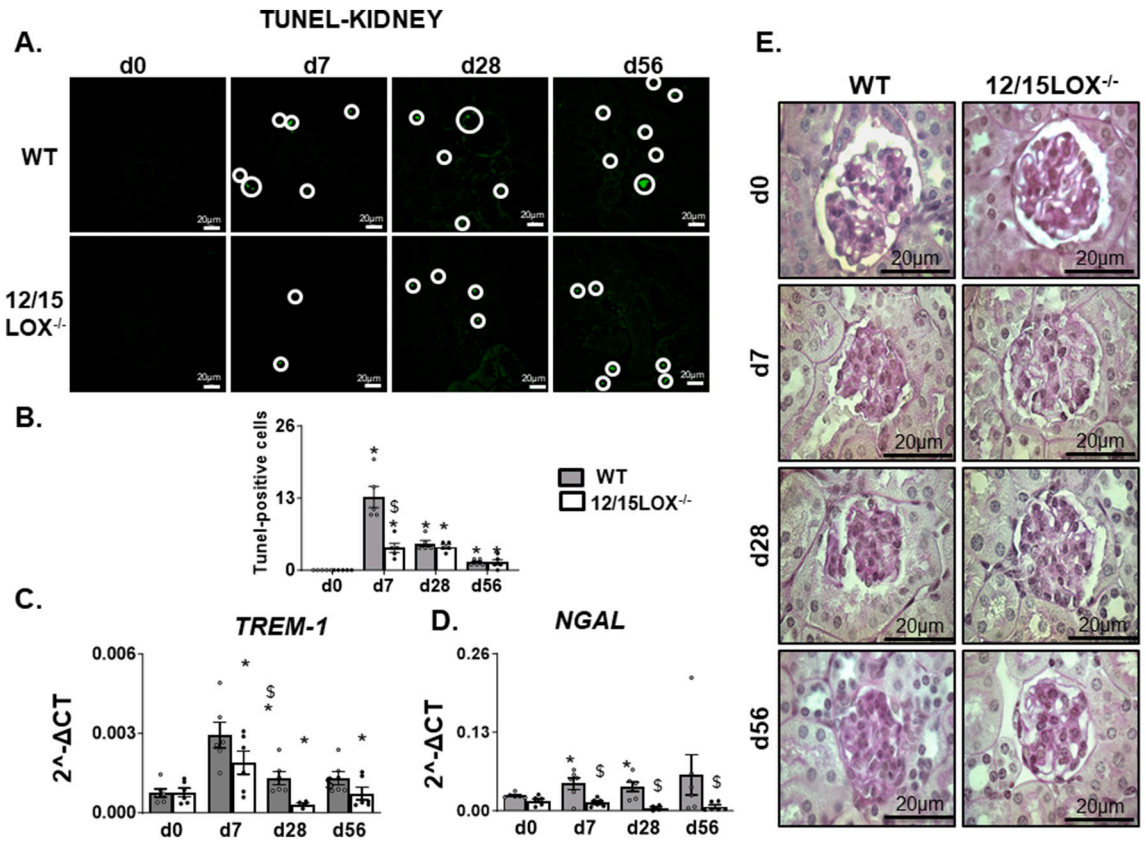

Fig. 7. Deletion of 12/15 LOX leads to decreased kidney apoptosis and kidney inflammation marmer following pressure overload.
A. Representative images of TUNEL staining of the kidney at d7, d28, and d56 post-TAC, representing a decrease in apoptotic cells (TUNEL positive cell: green) in12/15LOX$^{-/-}$ mice compared with WT mice (magnification 40×, scale bar indicates 20 μm). Images are representative of 8 fields/slides. n=4 mice slides/group. **B**. Bar graph representing TUNEL positive cells. mRNA expression of **C.** TREM and **D.** NGAL post-TAC in WT and 12/15LOX$^{-/-}$ mice. Data information: Comparisons between groups at time points were done using ordinary two-way ANOVA with multiple-comparisons test (Number of mice WT: d0, n=4; d7, n=4; d28, n=4; d56, n=4; Number of mice 12/15LOX$^{-/-}$: d0, n=4; d7, n=4; d28, n=4; d56, n=4). Values are represented as mean±SEM; *n*=5 mice *p<0.05 vs. d0 respective control, $p<0.05 vs. WT at respective time points. **E**. 100× magnification images of periodic acid Schiff's (PAS) stained kidney glomerulus at d0 and at d7, d28, and d56 post-TAC. Images are representative of 8 fields/slides. n=4 individual mouse slides/group. (For interpretation of the references to color in this figure legend, the reader is referred to the web version of this article.)

4. Discussion

Cardiac remodeling is a pathological process characterized by changes in the size, shape, and function of the left ventricle leading to heart failure [28]. The surgical coronary artery ligation is intense stress on the myocardium leading to necrosis in the infarcted area with subsequent heart failure. In contrast, TAC causes chronic, low-grade insult to the heart, leading to pressure-overload-directed heart failure [29]. Therefore, the pathway and timing of remodeling are relatively different. In the TAC of risk-free mice, we revealed two distinct processes: early adaptive remodeling (until week 1) and chronic maladaptive remodeling (after week 1–2 months) marked with a distinct set of lipid mediators. Our previous reports indicate that 12/15LOX deficiency is protective in ischemic remodeling post-MI and survival [17]. In the current study, we investigated the role of 12/15LOX in adaptive and maladaptive cardiac remodeling in a pressure overload mouse model. Our results indicate that 12/15LOX deficiency in pressure overload 1) improves ventricular function and reduces ventricular hypertrophy; 2) lowers 12-HETE, prostaglandins, with a marked increase of 11,12 EpETE in the heart; 3) upregulates miR 7a-5p and diminishes miR-26a-5p during chronic, maladaptive remodeling; 4) reduces intracardiac interstitial fibrosis with adverse vascular remodeling during the maladaptive response, and 5) reduces renal injury. In summary, 12/15LOX deletion improved ventricular function by decreasing proinflammatory 12-HETE and increasing SPMs and CYP-derived 11,12 EpETE.

Both proinflammatory and SPMs are critical in cardiac repair and remodeling [30]. Our previous studies have indicated that deletion of 12/15LOX not only limited pro-inflammatory 12- HETE but shifts the lipid metabolism pathways towards CYP-mediated AA metabolism, increasing the EETs [17]. Along with 12-HETE, PGD_2, PGE_2, and $PGF_{2\alpha}$ are proinflammatory lipid mediators. In contrast, SPMs are pro-resolving and released in response to stimuli or injury [31–36]. PGs are mediated through the COX-1/2 pathway, deteriorate ECM remodeling, and aggravate cytokine response. The 12/15lipoxygenase (ALOX15) also produces 12(*S*)- and 15(*S*)-HETE, but the relative proportion of HETEs generated is species-specific. In humans, 12/15LOX produces 10 % 12(*S*)-HETE vs. 90 % 15(*S*)-HETE, while in mice, the enzyme produces 90 % 12(*S*)-HETE vs. 10 % 15(*S*)-HETE [20]. 12/15LOX is present in several infiltrating cells, including macrophages and neutrophils, which elevates 12-HETE levels across tissues under pathological conditions via mobilization and presence of these infiltrating cells [20]. In the current study, we observed that PGs and 12-HETE levels were elevated during adaptive remodeling, but during maladaptive remodeling, these levels peaked, indicating a pronounced inflammation in WT mice. Deletion of 12/15LOX diminished both PGs and 12-HETE levels. Instead, there is an increase in the EpETEs, specifically 11,12 EpETEs, generated via epoxidation of EPA. Deleting 12/15LOX in mice polarizes macrophages towards a pro-resolving phenotype by diminishing 12-HETE and elevating EETs levels following ischemic injury [17]. In case of pressure overload model as we observed lower

levels of proinflammatory mediator in 12/15LOX deletion mice, limiting adverse remodeling and improving cardiac function.

Our TAC model also found the novel adversarial effect of 12/15LOX deletion. To our surprise, we found adverse vascular remodeling with aberrant CD31 staining within LV, with intense peri-vascular fibrosis on picrosirius red staining in 12/15LOX$^{-/-}$ mice during the chronic, maladaptive period. Though Arg-1 is known to be a pro-resolving cytokine, it plays a positive role in inducing vascular fibrosis leading to elevated vascular stiffness and decreased arterial compliance, which is recognized as an important and independent cardiovascular risk factor [37,38]. The increase in Arg-1 in 12/15LOX$^{-/-}$ mice serve a dual role and is likely to be a compensatory mechanism for the long-term 12/15LOX deletion in pressure overload. Further studies of neointimal formation investigating this phenomenon are warranted in chronic remodeling.

Both chronic heart failure (CHF) and chronic kidney disease (CKD) are known to cause the elaboration of several proinflammatory mediators that can be detected at high concentrations in the tissues and bloodstream. Renal dysfunction is common in heart failure patients and confers a worse prognosis [39,40]. CHF and CKD are governed by the elaboration of proinflammatory cytokines leading to multi-organ inflammation and contributing morbidity in pressure overload mice. TREM-1 expression peaked during adaptive cardiac remodeling, which stimulates neutrophil and monocyte-mediated inflammatory responses. NGAL is a potent acute kidney injury biomarker immediately elevated due to the acute inflammation in the kidney [41]. Unlike TREM, NGAL keeps upregulating during the maladaptive cardiac response in WT mice. 12/15LOX deletion downregulated TREM and NGAL expression, indicating reduced renal inflammation.

4.1. Study limitations

Our study has several limitations. First, although we show a surprising novel finding of adverse vascular remodeling in chronic stages after TAC in 12/15LOX$^{-/-}$ mice. We did not investigate in detail the upstream or downstream effect of this finding. Second, this study aimed to investigate the role of 12/15 LOX in cardiac remodeling rather than focusing on the vasculature. Third, although not necessarily a limitation, we did not find an improved survival outcome in 12/15 LOX knockout compared to the wild type in TAC. This is despite the clinical phenotype seen on echocardiogram and necropsy with LV systolic dysfunction, LV dilatation, lung edema, and less interstitial fibrosis of the myocardium. This may be due to the compensatory mechanism of other lipid mediator enzymes that lead to a pathologic increase in peri-vascular fibrosis. Further studies should be performed to investigate this dual phenotype. Fourth, we have only used male mice in the presented report, thus female mice may give different results. Lastly, we used a genetic deletion of 12/15 LOX without other traditional risk factors seen in humans. Heart failure can be a complex clinical and heterogenous phenomenon involving various risk factors, including obesity hypertension and diabetes. In our study, however, we only modified one risk factor, the 12/15LOX, thus should be interpreted accordingly.

In conclusion, deficiency of 12/15 LOX serves a dual role in early adaptive interstitial remodeling with both long-term protective effects on cardiac hypertrophy and cardiac fibrosis and detrimental adverse vascular remodeling during later maladaptive phase after pressure overload.

Acknowledgment and funding

This work was supported in part from the National Institutes of Health HL132989 and HL144788 to GVH.

Declaration of competing interest

The authors declare the following financial interests/personal relationships which may be considered as potential competing interests:

Ganesh Halade reports financial support was provided by National Heart Lung and Blood Institute Division of Cardiovascular Sciences.

Appendix A. Supplementary data

Supplementary data to this article can be found online at https://doi.org/10.1016/j.jmccpl.2023.100046.

References

[1] Tsao CW, Aday AW, Almarzooq ZI, Alonso A, Beaton AZ, Bittencourt MS, et al. Heart disease and stroke statistics-2022 update: a report from the American Heart Association. Circulation 2022;145(8):e153–639.
[2] Roth GA, Mensah GA, Johnson CO, Addolorato G, Ammirati E, Baddour LM, et al. 1990–2019: update from the GBD 2019 study. J Am Coll Cardiol 2020;76(25):2982–3021.
[3] Heidenreich PA, Bozkurt B, Aguilar D, Allen LA, Byun JJ, Colvin MM, et al. 2022 AHA/ACC/HFSA guideline for the management of heart failure: executive summary: a report of the American College of Cardiology/American Heart Association Joint Committee on Clinical Practice Guidelines. Circulation 2022;145(18):e876–94.
[4] Halade GV, Lee DH. Inflammation and resolution signaling in cardiac repair and heart failure. EBioMedicine 2022;79:103992.
[5] S.P. Murphy, R. Kakkar, C.P. McCarthy, J.L. Januzzi, Inflammation in Heart Failure, JACC State-of-the-Art Review 75(11) (2020) 1324–1340.
[6] Rao A, Gupta A, Kain V, Halade GV. Extrinsic and intrinsic modulators of inflammation-resolution signaling in heart failure. Am J Physiol Heart Circ Physiol 2023;325(3):H433–h448.
[7] Tourki B, Halade GV. Heart failure syndrome with preserved ejection fraction is a metabolic cluster of non-resolving inflammation in obesity. Front Cardiovasc Med 2021;8:695952.
[8] Pullen AB, Jadapalli JK, Rhourri-Frih B, Halade GV. Re-evaluating the causes and consequences of non-resolving inflammation in chronic cardiovascular disease. Heart Fail Rev 2020;25(2):381–91.
[9] Rockman HA, Ross RS, Harris AN, Knowlton KU, Steinhelper ME, Field LJ, et al. Segregation of atrial-specific and inducible expression of an atrial natriuretic factor transgene in an in vivo murine model of cardiac hypertrophy. Proc Natl Acad Sci USA 1991;88(Medical Sciences):8277–81.
[10] Laroumanie F, Douin-Echinard V, Pozzo J, Lairez O, Tortosa F, Vinel C, et al. CD4+ T cells promote the transition from hypertrophy to heart failure during chronic pressure overload. Circulation 2014;129(21):2111–24.
[11] Martini E, Kunderfranco P, Peano C, Carullo P, Cremonesi M, Schorn T, et al. Single-cell sequencing of mouse heart immune infiltrate in pressure overload-driven heart failure reveals extent of immune activation. Circulation 2019;140(25):2089–107.
[12] Patel B, Bansal SS, Ismahil MA, Hamid T, Rokosh G, Mack M, et al. CCR2(+) monocyte-derived infiltrating macrophages are required for adverse cardiac remodeling during pressure overload. JACC Basic Transl Sci 2018;3(2):230–44.
[13] Revelo XS, Parthiban P, Chen C, Barrow F, Fredrickson G, Wang H, et al. Cardiac resident macrophages prevent fibrosis and stimulate angiogenesis. Circ Res 2021;129(12):1086–101.
[14] Halade GV, Kain V, Hossain S, Parcha V, Limdi NA, Arora P. Arachidonate 5-lipoxygenase is essential for biosynthesis of specialized pro-resolving mediators and cardiac repair in heart failure. Am J Physiol Heart Circ Physiol 2022;323(4):H721–h737.
[15] Halade GV, Kain V, Ingle KA. Heart functional and structural compendium of cardiosplenic and cardiorenal networks in acute and chronic heart failure pathology. American Journal of Physiology-Heart and Circulatory Physiology 2018;314(2):H255–67.
[16] Kain V, Ingle KA, Rajasekaran NS, Halade GV. Activation of EP4 receptor limits transition of acute to chronic heart failure in lipoxygenase deficient mice. Theranostics 2021;11(6):2742–54.
[17] Kain V, Ingle KA, Kabarowski J, Barnes S, Limdi NA, Prabhu SD, et al. Genetic deletion of 12/15 lipoxygenase promotes effective resolution of inflammation following myocardial infarction. J Mol Cell Cardiol 2018;118:70–80.
[18] Hernandez-Perez M, Chopra G, Fine J, Conteh AM, Anderson RM, Linnemann AK, et al. Inhibition of 12/15-lipoxygenase protects against β-cell oxidative stress and glycemic deterioration in mouse models of type 1 diabetes. Diabetes 2017;66(11):2875–87.
[19] Huo Y, Zhao L, Hyman MC, Shashkin P, Harry BL, Burcin T, et al. Critical role of macrophage 12/15-lipoxygenase for atherosclerosis in apolipoprotein E-deficient mice. Circulation 2004;110(14):2024–31.
[20] Dobrian AD, Lieb DC, Cole BK, Taylor-Fishwick DA, Chakrabarti SK, Nadler JL. Functional and pathological roles of the 12- and 15-lipoxygenases. Prog Lipid Res 2011;50(1):115–31.
[21] Conrad DJ, Kuhn H, Mulkins M, Highland E, Sigal E. Specific inflammatory cytokines regulate the expression of human monocyte 15-lipoxygenase. Proc Natl Acad Sci U S A 1992;89(1):217–21.
[22] Cyrus T, Witztum JL, Rader DJ, Tangirala R, Fazio S, Linton MF, et al. Disruption of the 12/15-lipoxygenase gene diminishes atherosclerosis in apo E-deficient mice. J Clin Invest 1999;103(11):1597–604.

[23] Houser SR, Margulies KB, Murphy AM, Spinale FG, Francis GS, Prabhu SD, et al. Animal models of heart failure: a scientific statement from the American Heart Association. Circ Res 2012;111(1):131–50.
[24] Lopez EF, Kabarowski JH, Ingle KA, Kain V, Barnes S, Crossman DK, et al. Obesity superimposed on aging magnifies inflammation and delays the resolving response after myocardial infarction. Am J Physiol Heart Circ Physiol 2015;308(4):H269–80.
[25] Halade GV, Kain V, Black LM, Prabhu SD, Ingle KA. Aging dysregulates D- and E-series resolvins to modulate cardiosplenic and cardiorenal network following myocardial infarction. Aging (Albany NY) 2016;8(11):2611–34.
[26] Halade GV, Kain V, Ingle KA, Prabhu SD. Interaction of 12/15-lipoxygenase with fatty acids alters the leukocyte kinetics leading to improved postmyocardial infarction healing. American Journal of Physiology-Heart and Circulatory Physiology 2017;313(1):H89–102.
[27] Halade GV, Kain V. Obesity and cardiometabolic defects in heart failure pathology. Compr Physiol 2017;7(4):1463–77.
[28] Cohn JN, Ferrari R, Sharpe N. Cardiac remodeling—concepts and clinical implications: a consensus paper from an international forum on cardiac remodeling. J Am Coll Cardiol 2000;35(3):569–82.
[29] de Almeida AC, van Oort RJ, Wehrens XH. Transverse aortic constriction in mice. J Vis Exp 2010;38.
[30] Halade GV, Norris PC, Kain V, Serhan CN, Ingle KA. Splenic leukocytes define the resolution of inflammation in heart failure. Science Signaling 2018;11(520):eaao1818.
[31] Halade GV, Kain V, Dillion C, Beasley M, Dudenbostel T, Oparil S, et al. Race-based and sex-based differences in bioactive lipid mediators after myocardial infarction. ESC Heart Fail 2020;7(4):1700–10.
[32] Fosshaug LE, Colas RA, Anstensrud AK, Gregersen I, Nymo S, Sagen EL, et al. Early increase of specialized pro-resolving lipid mediators in patients with ST-elevation myocardial infarction. EBioMedicine 2019;46:264–73.
[33] Ricciotti E, FitzGerald GA. Prostaglandins and inflammation. Arterioscler Thromb Vasc Biol 2011;31(5):986–1000.
[34] Kayama Y, Minamino T, Toko H, Sakamoto M, Shimizu I, Takahashi H, et al. Cardiac 12/15 lipoxygenase-induced inflammation is involved in heart failure. J Exp Med 2009;206(7):1565–74.
[35] Serhan CN. Pro-resolving lipid mediators are leads for resolution physiology. Nature 2014;510(7503):92–101.
[36] Serhan CN, Levy BD. Resolvins in inflammation: emergence of the pro-resolving superfamily of mediators. J Clin Invest 2018;128(7):2657–69.
[37] Bhatta A, Yao L, Xu Z, Toque HA, Chen J, Atawia RT, et al. Obesity-induced vascular dysfunction and arterial stiffening requires endothelial cell arginase 1. Cardiovasc Res 2017;113(13):1664–76.
[38] Toque HA, Nunes KP, Rojas M, Bhatta A, Yao L, Xu Z, et al. Arginase 1 mediates increased blood pressure and contributes to vascular endothelial dysfunction in deoxycorticosterone acetate-salt hypertension. Front Immunol 2013;4:219.
[39] Zannad F, Rossignol P. Cardiorenal syndrome revisited. Circulation 2018;138(9):929–44.
[40] Colombo PC, Ganda A, Lin J, Onat D, Harxhi A, Iyasere JE, et al. Inflammatory activation: cardiac, renal, and cardio-renal interactions in patients with the cardiorenal syndrome. Heart Fail Rev 2012;17(2):177–90.
[41] Fodor R, Grigorescu B, Veres M, Orlandea M, Badea J, Hlavathy K, et al. Plasma neutrophil gelatinase associated lipocalin (NGAL) - early biomarker for acute kidney injury in critically ill patients. J Crit Care Med (Targu Mures) 2015;1(4):154–61.